

# Superplastic deformation mechanism of an ultrafine-grained aluminum alloy produced by friction stir processing

Z.Y. Ma <sup>a,\*</sup>, F.C. Liu <sup>a</sup>, R.S. Mishra <sup>b</sup>

<sup>a</sup> Shenyang National Laboratory for Materials Science, Institute of Metal Research, Chinese Academy of Sciences, 72 Wenhua Road, Shenyang 110016, China

<sup>b</sup> Center for Friction Stir Processing and Department of Materials Science and Engineering, Missouri University of Science and Technology, Rolla, MO 65409, USA

Received 3 February 2010; received in revised form 28 April 2010; accepted 1 May 2010  
Available online 4 June 2010

## Abstract

An ultrafine-grained (UFG) Al–4Mg–1Zr alloy with a grain size of  $\sim 0.7 \mu\text{m}$  with predominantly high-angle boundaries of 97% was produced by friction stir processing (FSP). The UFG Al–4Mg–1Zr retained submicrometer grains even after static annealing at 425 °C, and exhibited excellent superplasticity at 175–425 °C. High strain rate and low-temperature superplasticity of >1200% were observed at  $1 \times 10^{-2}$ – $1 \times 10^{-1} \text{ s}^{-1}$  and 300–350 °C. Even at 425 °C, a superplasticity of 1400% was achieved at  $1 \text{ s}^{-1}$ . A linear relationship between  $\log \dot{\epsilon}_{\text{opti}}$  and  $T$  was observed (where  $\dot{\epsilon}_{\text{opti}}$  is the optimum strain rate, and  $T$  is the temperature). The analyses on the superplastic data revealed the presence of threshold stress, a stress exponent of 2, an inverse grain size dependence of 2, and an activation energy of 142 kJ mol<sup>-1</sup>. This indicated that the dominant deformation mechanism was grain boundary sliding, which was controlled by lattice diffusion. Based on this notion, a constitutive equation has been developed. A new superplastic deformation mechanism map for FSP aluminum alloys is proposed.

© 2010 Acta Materialia Inc. Published by Elsevier Ltd. All rights reserved.

**Keywords:** Superplasticity; Friction stir processing; Aluminum alloys; Ultrafine-grained microstructure

## 1. Introduction

Superplasticity refers to the ability of materials to exhibit high uniform elongation when pulled in tension. From the viewpoint of practical industrial fabrication, it is highly desirable to perform superplastic forming at higher strain rates and/or lower temperatures. A higher forming rate of  $>1 \times 10^{-2} \text{ s}^{-1}$  is very attractive for current industrial fabrication techniques because one of the drawbacks with existing superplastic forming technology is its low forming rate, typically  $10^{-5}$ – $10^{-3} \text{ s}^{-1}$  [1]. On the other hand, a lower forming temperature would save energy, prevent grain growth, and reduce cavitation level and solute loss

from the surface layer, thereby maintaining superior post-forming properties [2].

In the past few years, much research has been devoted to producing fine-grained aluminum alloys exhibiting high strain rate superplasticity (HSRS) and/or low-temperature superplasticity (LTSP), by using thermomechanical treatment (TMT) [3–5], equal channel angular pressing (ECAP) [6–9], high-pressure torsion (HPT) [10], multiaxial alternative forging (MAF) [11], and accumulative roll bonding (ARB) [12].

Friction stir processing (FSP) is a relatively new processing technique for producing fine-grained aluminum alloys exhibiting HSRS and/or LTSP. This has led to considerable research interest in superplastic behavior of FSP aluminum alloys. In the past few years, a number of aluminum alloys, such as 7075Al, 7050Al, 2024Al, 5083Al, A356,

\* Corresponding author. Fax: +86 24 83978908.  
E-mail address: [zym@imr.ac.cn](mailto:zym@imr.ac.cn) (Z.Y. Ma).

Al–4Mg–1Zr, Al–Mg–Sc and Al–Zn–Mg–Sc, have been subjected to FSP and superplasticity investigations [13–23].

It is important to develop a constitutive equation of superplastic flow for FSP aluminum alloys. The steady-state deformation of polycrystalline materials at elevated temperatures is usually analyzed through the equation [25–28]:

$$\dot{\epsilon} = A \frac{D_0 E b}{kT} \exp\left(-\frac{Q}{RT}\right) \left(\frac{b}{d}\right)^p \left(\frac{\sigma - \sigma_0}{E}\right)^n, \quad (1)$$

where  $\dot{\epsilon}$  is the strain rate,  $A$  is a constant,  $D_0$  is the pre-exponential factor for diffusion,  $E$  is the Young's modulus,  $b$  is the Burger's vector,  $k$  is the Boltzmann's constant,  $T$  is the absolute temperature,  $Q$  is the activation energy dependent on the rate-controlling process,  $R$  is the gas constant,  $d$  is the grain size,  $\sigma$  is the applied stress, and  $\sigma_0$  is the threshold stress. Three variables,  $n$ ,  $p$  and  $Q$ , are the most important for determining the deformation mechanism.

A number of fine-grained FSP aluminum alloys (grain sizes 1–10  $\mu\text{m}$ ) exhibit HSRS [13–19]. Surface observations have revealed evidence of GBS. The constitutive equations have been described in the form of [14,16,18]:

$$\dot{\epsilon} = A \frac{D_0 E b}{kT} \exp\left(-\frac{84000}{RT}\right) \left(\frac{b}{d}\right)^2 \left(\frac{\sigma - \sigma_0}{E}\right)^2. \quad (2)$$

The coefficient  $A$  is in the range of 700–1400, which suggests that the kinetics of grain boundary sliding (GBS), which dominate the deformation in the FSP materials, is higher than that in conventionally processed materials [27]. The deformation mechanism is GBS controlled by grain boundary diffusion.

LTSP has been obtained in several FSP ultrafine-grained (UFG) aluminum alloys, such as 7075Al, Al–4Mg–1Zr, Al–Mg–Sc and Al–Zn–Mg–Sc [20–24]. The optimum strain rate, maximum elongation and strain rate sensitivity shifts to higher values with increasing temperature. Abnormal grain growth (AGG) usually occurs in the UFG alloys at elevated temperatures, resulting in the disappearance of superplasticity. Surface observation of the deformed specimens indicates that GBS occurs during LTSP. Marker line offset measurements have shown that the contribution of GBS to the total strain for FSP UFG Al–Mg–Sc exceeded 50% even at 175  $^{\circ}\text{C}$  [24]. Despite a number of LTSP studies on the FSP UFG aluminum alloys, fundamental understanding of the deformation mechanism is still poor. Stress exponent, grain size exponent and activation energy should be characterized to clarify the deformation mechanism. A constitutive equation for the UFG alloys is also needed for superplastic forming in practical industrial fabrication.

Recently, a UFG Al–4Mg–1Zr alloy with a grain size of 0.7  $\mu\text{m}$  was produced via FSP under a low heat input using a small tool [22]. It was reported that this UFG Al–4Mg–1Zr exhibited superplasticity of 240% at a low temperature of 175  $^{\circ}\text{C}$ , corresponding to 0.48 $T_m$ , where  $T_m$  is the absolute melting temperature of aluminum. This was the first

report of superplasticity at temperatures below 0.5 $T_m$  for aluminum alloys. Irrespective of good superplasticity at lower temperatures, superplastic tensile tests over a wide temperature range, detailed microstructural examinations and superplastic data analyses on the FSP UFG Al–4Mg–1Zr are still lacking.

In this work, the superplastic behavior of the FSP UFG Al–4Mg–1Zr was investigated over a wide temperature range of 175–425  $^{\circ}\text{C}$  and strain rates of  $5 \times 10^{-5}$ –3  $\text{s}^{-1}$ . The purpose of this study is: (i) to examine the boundary characteristics and thermal stability of the FSP UFG Al–4Mg–1Zr; (ii) to evaluate the superplastic behavior of the FSP UFG Al–4Mg–1Zr at elevated temperatures; and (iii) last, but most importantly, through clarifying the stress exponent, grain size exponent and activation energy, to develop a constitutive equation for UFG aluminum alloys and identify the deformation mechanism.

## 2. Experimental

Al–4Mg–1Zr was obtained as a 10 mm  $\times$  20 mm extruded bar. Fabrication of the extruded bar has been described in detail in previous works [29,30]. Single-pass FSP was conducted on the extruded bar along the extrusion direction at a tool rotation rate of 600 rpm and a tool traverse speed of 25.4 mm  $\text{min}^{-1}$ . A tool with a shoulder 12 mm in diameter and a threaded cylindrical pin 4 mm in diameter and 4 mm in length was used.

The specimens for microstructural examination were cross-sectioned perpendicular to the FSP direction. Microstructural characterization and analysis were carried out using transmission electron microscopy (TEM) and scanning electron microscopy (SEM, Hitachi S-3400N). Thin foils for TEM were prepared using jet polishing techniques. Jet polishing was conducted at  $-25$   $^{\circ}\text{C}$  using a solution of 20%  $\text{HNO}_3$  + 80% methanol (by vol.). The average grain size in the FSP sample was determined by the mean linear intercept technique. The specimens for SEM were lightly electropolished to produce a strain-free surface. Electron backscatter diffraction (EBSD) orientation maps (with a resolution of 80 nm) were obtained using a Zeiss Supra 35, operated at 20 kV, and interfaced to an HKL Channel EBSD system. The indexing rate was 91%. A standard noise reduction technique was applied before calculating the misorientation angles. Owing to the limited angular resolution, misorientations less than  $2^{\circ}$  were not considered.

To check the thermal stability of the ultrafine grains produced by FSP, small specimens with a dimension of 10  $\times$  10  $\times$  10  $\text{mm}^3$  cut from the FSP sample were statically annealed for 20 min at temperatures ranging from 175 to 425  $^{\circ}\text{C}$ , and then water quenched to provide microstructure information of the FSP sample just before tensile tests at various temperatures.

Mini tensile specimens with a gauge length of 1.3 mm were electrodischarge-machined from the FSP region in the transverse direction, ground and polished to a final thickness of  $\sim$ 0.5 mm using a 1  $\mu\text{m}$  polishing paste. Constant crosshead

speed tensile tests were conducted using a computer-controlled, custom-built mini tensile tester. The surfaces of deformed specimens were subjected to SEM examination.

### 3. Results

#### 3.1. Microstructure

Fig. 1 shows TEM micrographs of as-extruded and FSP Al–4Mg–1Zr samples. The microstructure of the extruded sample was characterized by predominant low-angle grain boundaries (LAGBs) with grains/subgrains aligned along the extrusion direction [29], and with nonuniform grain size (Fig. 1a). For the FSP sample, the microstructure was characterized by uniform and equiaxed recrystallized grains with predominant high-angle grain boundaries (HAGBs) (Fig. 1b) and an average grain size of  $\sim 0.7 \mu\text{m}$  [22]. A high density of  $\text{Al}_3\text{Zr}$  dispersoids with sizes ranging from 5 to 20 nm were uniformly distributed in the aluminum matrix (Fig. 1c).

The frequency distribution of boundary misorientation angles for the FSP Al–4Mg–1Zr is shown in Fig. 2. The fraction of HAGBs was measured to be 97%. For comparison, the theoretical distribution of grain boundary misorientation angles for a random polycrystal of cubic

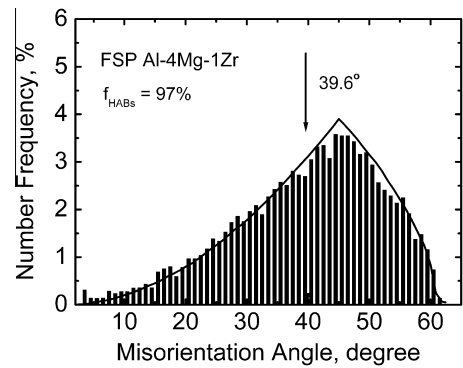


Fig. 2. Grain boundary misorientation angle distribution for FSP Al–4Mg–1Zr.

structure [31] is also shown in Fig. 2 by a black solid line. It is seen that the misorientation distribution for the FSP Al–4Mg–1Zr shows a close match with the theoretical distribution.

#### 3.2. Thermal stability of ultrafine grains

Fig. 3 shows the typical grain microstructure of the FSP Al–4Mg–1Zr after static annealing for 20 min at 175 and 425 °C. It is clear that the fine-grained structure did not

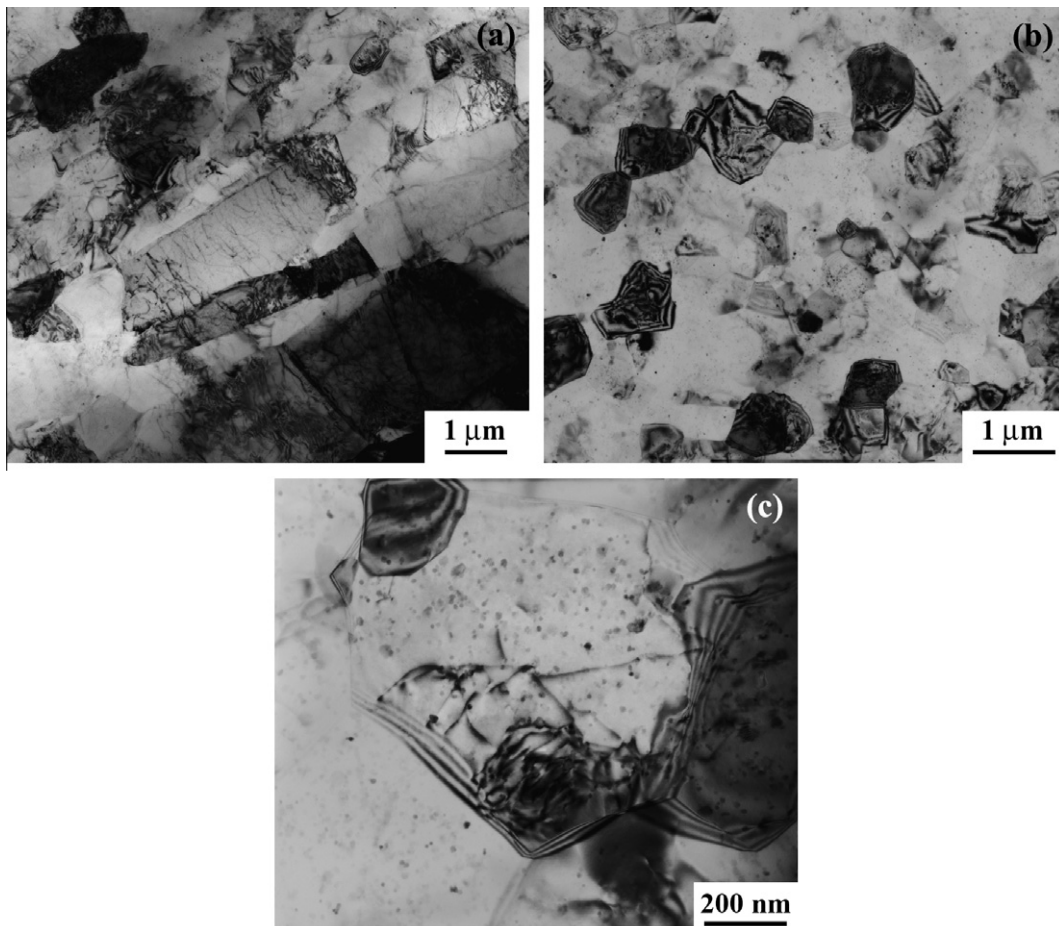


Fig. 1. TEM images showing grain structure and dispersoid distribution in (a) as-extruded Al–4Mg–1Zr, (b) and (c) FSP Al–4Mg–1Zr.

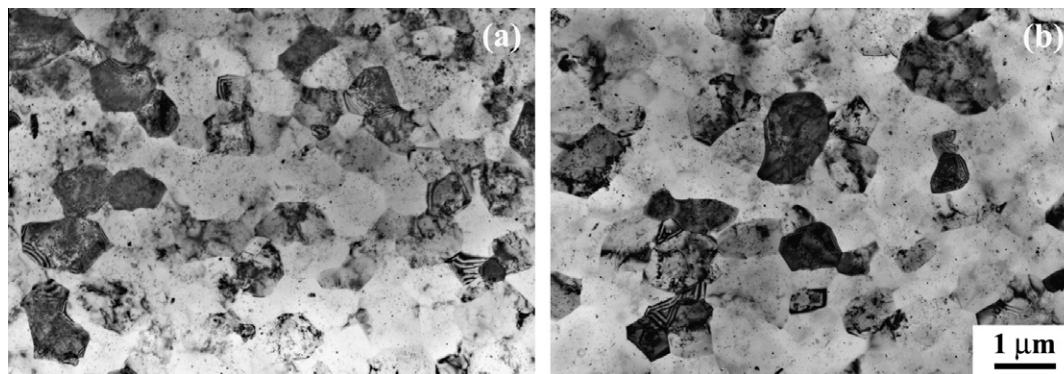


Fig. 3. Typical microstructures for FSP Al-4Mg-1Zr after static annealing at (a) 175 °C and (b) 425 °C.

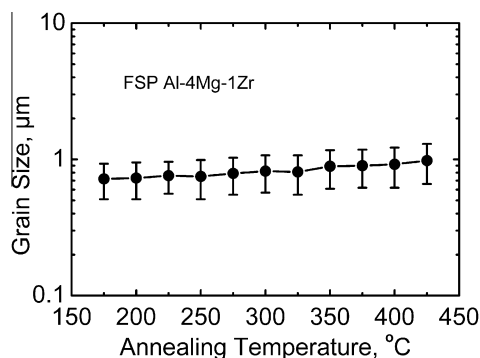


Fig. 4. Grain size as a function of annealing temperature for FSP Al-4Mg-1Zr.

exhibit an obvious coarsening after static annealing and the equiaxed grains were retained. The average grain sizes were 0.72 and 0.98 μm for the annealing temperatures of 175 and 425 °C, respectively. Fig. 4 shows the variation of the average grain size with the static annealing temperature for the FSP Al-4Mg-1Zr. It is apparent that the FSP Al-4Mg-1Zr exhibited excellent thermal stability and retained sub-micrometer grains even at an annealing temperature of 425 °C.

It should be noted that the  $\text{Al}_3\text{Zr}$  dispersoids did not exhibit noticeable coarsening after static annealing even at 425 °C (Fig. 5). These precipitates were still of spherical shape and extremely fine, with a size range of 5–20 nm, and

homogeneously distributed throughout the matrix (Fig. 5). It is believed that these coherent  $\text{Al}_3\text{Zr}$  dispersoids were effective in pinning the grain boundaries.

### 3.3. Superplastic behavior

The overall superplastic data are presented in three sub-groups based on the observed trend between optimum strain rate and strain rate with temperature. The three temperature ranges are 175–250, 275–350 and 375–425 °C.

Figs. 6a, 7a and 8a show the variation of superplastic elongation with the initial strain rate in the temperature ranges of 175–250, 275–350 and 375–425 °C, respectively. The largest elongation and corresponding strain rates at various temperatures are summarized in Table 1. With increasing the temperature from 175 to 425 °C, the optimum strain rate and maximum ductility increased. At and above 300 °C, the maximum ductility of >1150% was obtained at the optimum strain rates. At 425 °C, the optimum strain rate was as high as  $1 \text{ s}^{-1}$ . Due to the limit of the ability of the tester, the tensile test at strain rates of  $>3 \text{ s}^{-1}$  could not be conducted. It is noted that high values of superplasticity of >1150% were obtained at high strain rates ( $1 \times 10^{-2}$ – $1 \times 10^{-1} \text{ s}^{-1}$ ) and low temperatures (300–350 °C).

Figs. 6b, 7b and 8b show the variation of flow stress (at a true strain of 0.1) with the initial strain rate in the temperature ranges of 175–250, 275–350 and 375–425,

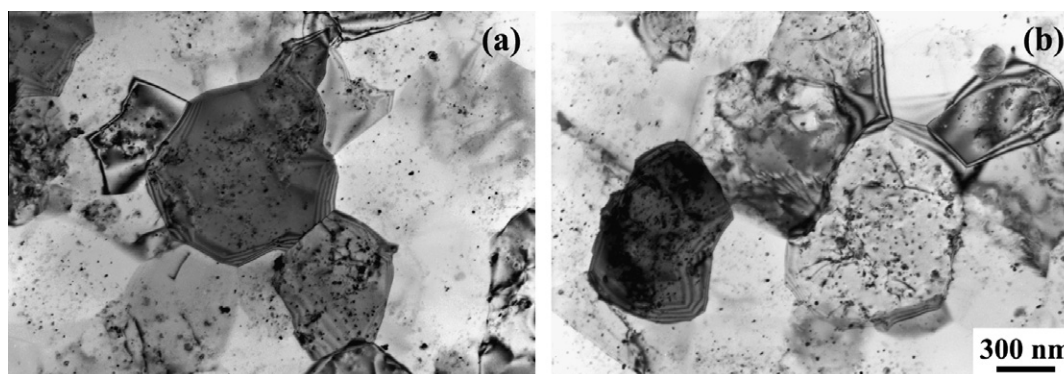


Fig. 5. Typical micrographs showing precipitates distribution for FSP Al-4Mg-1Zr after static annealing at (a) 175 °C and (b) 425 °C.

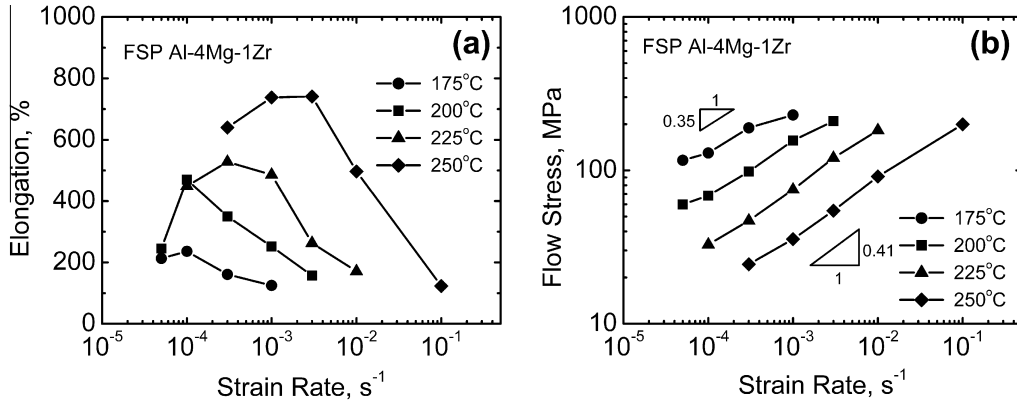


Fig. 6. Variation of (a) ductility and (b) flow stress with initial strain rate for testing temperatures of 175–250 °C for FSP Al-4Mg-1Zr.

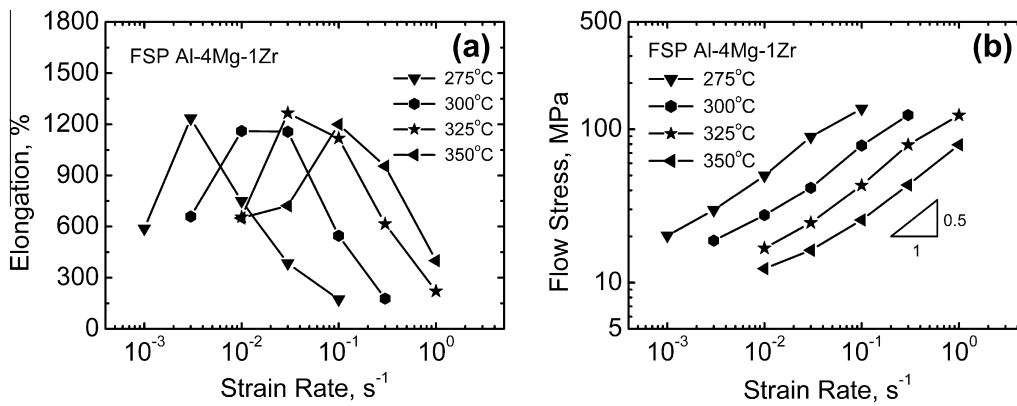


Fig. 7. Variation of (a) ductility and (b) flow stress with initial strain rate for testing temperatures of 275–350 °C for FSP Al-4Mg-1Zr.

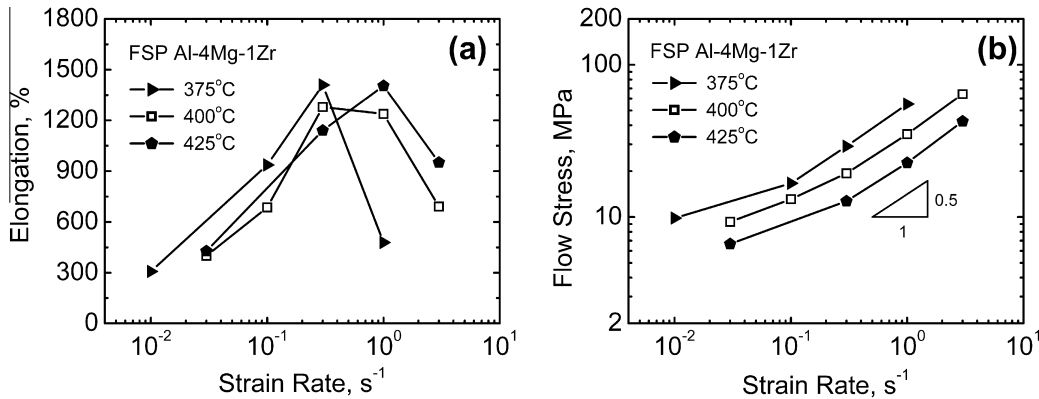


Fig. 8. Variation of (a) ductility and (b) flow stress with initial strain rate for testing temperatures of 375–425 °C for FSP Al-4Mg-1Zr.

respectively. The FSP Al-4Mg-1Zr exhibited the typical S-type stress–strain rate behavior characteristic of a super-plastic material. With increasing strain rate, the strain rate sensitivity  $m$  increased from lower values in region I to maximum values in region II, and then decreased in region III. At and above 350 °C, no decrease in the  $m$  value with the strain rate, i.e. a lack in region III, was observed due to the absence of experimental data at strain rate of  $\geq 1\text{--}3\text{ s}^{-1}$ . The maximum  $m$  values and corresponding strain rates are also summarized in Table 1. The maximum  $m$  values of

0.34, 0.36, 0.41 and 0.41 were observed at 175, 200, 225 and 250 °C, respectively. At and above 275 °C, the maximum  $m$  values of  $\sim 0.5$  were consistently observed. It is noted that the strain rates for the maximum ductility are consistent with those for the maximum  $m$  values.

### 3.4. Microstructure of deformed specimens

Fig. 9 shows the topography of the FSP Al-4Mg-1Zr specimens deformed to failure at the optimum strain rates

Table 1

A summary of superplastic properties of FSP Al–4Mg–1Zr at various temperatures.

Temperature (°C)	Optimum strain rate (s <sup>-1</sup> )	Maximum elongation (%)	Maximum <i>m</i> value	Strain rate range for maximum, <i>m</i> (s <sup>-1</sup> )
175	1 × 10 <sup>-4</sup>	240	0.34	1 × 10 <sup>-4</sup> – 3 × 10 <sup>-4</sup>
200	1 × 10 <sup>-4</sup>	470	0.36	1 × 10 <sup>-4</sup> – 1 × 10 <sup>-3</sup>
225	3 × 10 <sup>-4</sup>	530	0.41	3 × 10 <sup>-4</sup> – 3 × 10 <sup>-3</sup>
250	1 × 10 <sup>-3</sup> – 3 × 10 <sup>-3</sup>	740	0.41	1 × 10 <sup>-3</sup> – 1 × 10 <sup>-2</sup>
275	3 × 10 <sup>-3</sup>	1235	0.48	3 × 10 <sup>-3</sup> – 3 × 10 <sup>-2</sup>
300	1 × 10 <sup>-2</sup> – 3 × 10 <sup>-3</sup>	1160	0.53	3 × 10 <sup>-2</sup> – 1 × 10 <sup>-1</sup>
325	3 × 10 <sup>-2</sup>	1265	0.51	3 × 10 <sup>-2</sup> – 3 × 10 <sup>-1</sup>
350	1 × 10 <sup>-1</sup>	1200	0.49	1 × 10 <sup>-1</sup> –1
375	3 × 10 <sup>-1</sup>	1410	0.52	1 × 10 <sup>-1</sup> –1
400	3 × 10 <sup>-1</sup>	1280	0.52	3 × 10 <sup>-1</sup> –3
425	1	1405	0.52	3 × 10 <sup>-1</sup> –3

for various temperatures. Indication of GBS, evidenced by a surface-relief pattern, i.e. lifting or heaving of grain boundaries [32–34], was distinctly observed on the surfaces of the deformed specimens, even at a low temperature of 175 °C. With increasing the temperature from 175 to

300 °C (Fig. 9a and b), it appears that the size of the grains increased. However, increasing the temperature to 425 °C did not result in a further increase in the grain size (Fig. 9b and c). This is attributed to the shortened time for high-temperature exposure due to the increase in the strain rate. The grain structures of the FSP Al–4Mg–1Zr deformed to failure at various temperatures are shown in Fig. 10. It is noted that the grains were still equiaxed and fine after deformation. The average grain sizes were estimated to be 1.5, 2.1, 2.4 and 2.4 μm for the specimens deformed to failure at 175, 250, 350 and 425 °C, respectively. This indicates that the fine-grained structure of the FSP Al–4Mg–1Zr was relatively stable during superplastic deformation. Some level of cavitation was also observed in the failed specimens. It was documented that dynamic grain growth during the superplastic deformation was faster than static grain growth, and increased with increasing the strain and strain rate [35,36].

## 4. Discussion

### 4.1. Thermal stability

It was previously reported that the microstructure of FSP UFG Al–Zn–Mg–Sc, 7075 and Al–Mg–Sc alloys became highly unstable at 390, 400 and 350 °C, respectively [20,21,23,24]. However, ECAP and cold-rolled UFG

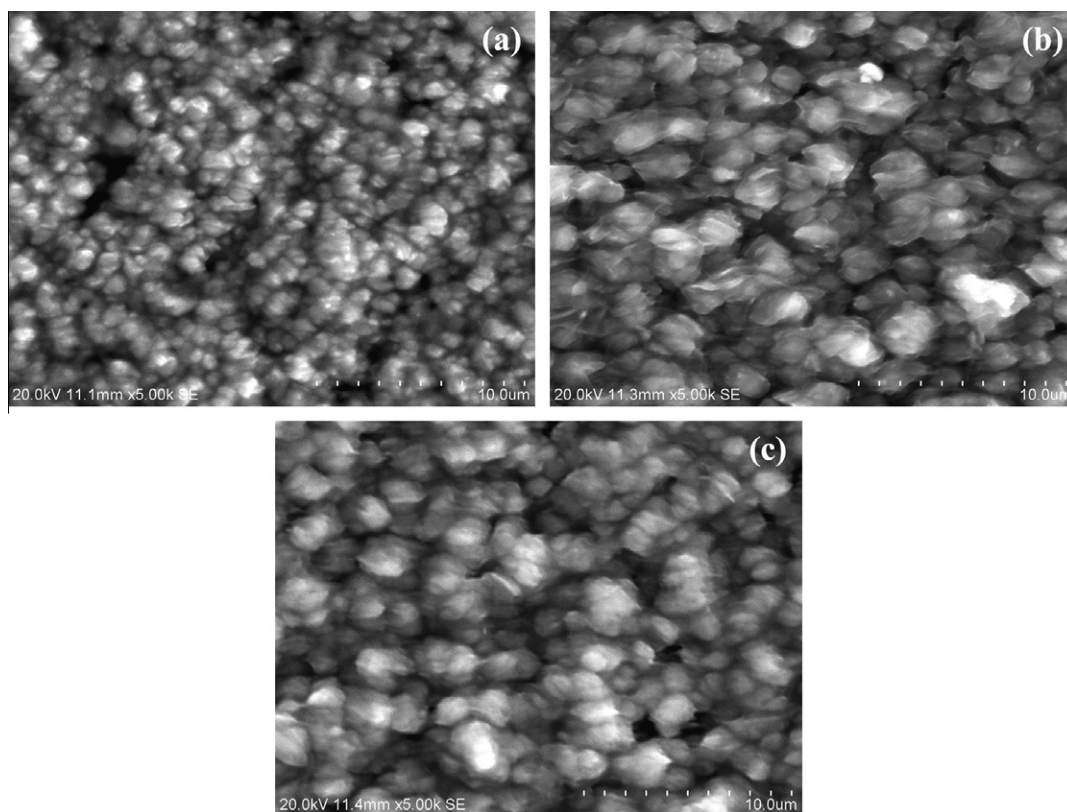


Fig. 9. Surface topography of tensile specimens near fracture tip deformed to failure at (a) 175 °C and 1 × 10<sup>-4</sup> s<sup>-1</sup>, (b) 300 °C and 1 × 10<sup>-2</sup> s<sup>-1</sup>, (c) 425 °C and 1 s<sup>-1</sup>.

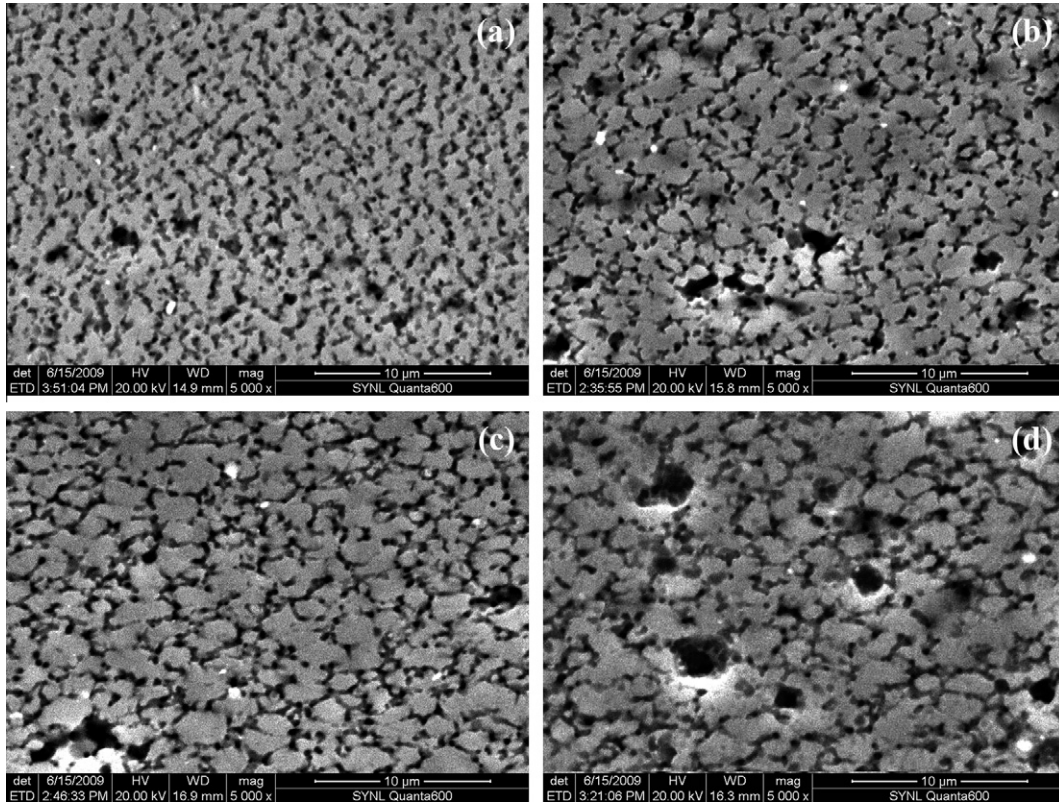


Fig. 10. Grain structures of tensile specimens near fracture tip deformed to failure at (a) 175 °C and  $1 \times 10^{-4} \text{ s}^{-1}$ , (b) 250 °C and  $3 \times 10^{-3} \text{ s}^{-1}$ , (c) 350 °C and  $1 \times 10^{-1} \text{ s}^{-1}$ , (d) 425 °C and  $1 \text{ s}^{-1}$ .

Al–Mg–Sc with similar compositions as FSP Al–Mg–Sc did not show AGG at testing temperatures as high as 450 °C [37,38].

For a volume fraction  $F_v$  of randomly distributed spherical particles of radius  $r$ , the Zener pinning pressure exerted by the particles on a boundary of energy  $\gamma$  was given by [39]:

$$P_z = \frac{3F_v\gamma}{2r}. \quad (3)$$

The Humphreys model [39,40] assumes that the microstructure consists of an assembly of equiaxed grains of mean equivalent radius  $\bar{R}$ , mean spherical particles radius  $\bar{r}$ , and mean boundary mobility  $\bar{M}$ . The growth rates of the grains in the presence of the particles are:

$$\frac{dR}{dt} = M \left( \frac{\bar{\gamma}}{\bar{R}} - \frac{\gamma}{R} - \frac{3F_v\gamma}{r} \right) \quad (4)$$

$$\text{and } \frac{d\bar{R}}{dt} = \bar{M}\bar{\gamma} \left( \frac{1}{4\bar{R}} - \frac{3F_v}{r} \right), \quad (5)$$

where  $dR/dt$  and  $d\bar{R}/dt$  are the growth rates of the grain and surrounding grains. Eqs. (4) and (5) predict that both low boundary mobility and energy are beneficial to decreasing the grain-coarsening rates. The FSP aluminum alloys are characterized by a high ratio of HAGBs, whose mobility and energy was generally higher than that of the LAGBs [39,41]. Therefore, it is not surprising that the grain-coarsening rate of the FSP alloys is higher than that

of ECAP and cold-rolled alloys, which contain a lower ratio of the HAGB.

For the FSP Al–4Mg–1Zr, although the number fraction of the HAGB was 97%, the UFG microstructure was stable up to 425 °C. This is attributed to following two factors. First, based on the higher Zr content of 1 wt.%, the volume fraction of the pinning  $\text{Al}_3\text{Zr}$  particles in the FSP Al–4Mg–1Zr was much higher than that in other FSP aluminum alloys [20,21,23,37,38]. This was verified by TEM observations (Fig. 1c). Second, the sizes of the  $\text{Al}_3\text{Zr}$  particles were very fine, ranging from 5 to 20 nm. Based on these factors, the  $F_v/r$  is extremely high in the FSP Al–4Mg–1Zr. Furthermore, the  $\text{Al}_3\text{Zr}$  particles generally exhibit a coherent relationship with the aluminum matrix. For the coherent particles, the Zener pinning pressure was computed to be 4 × greater than that predicted by Eq. (3) [42]. Therefore, the FSP Al–4Mg–1Zr exhibited excellent thermal stability.

#### 4.2. Correlation between optimum strain rate and deformation temperature

Eq. (1) predicts that the increase in the testing temperature results in an increase in the strain rate if the grain size is kept constant. However, for most fine-grained aluminum alloys, such an increasing trend was rarely observed over a wide range of the temperatures due to the remarkable grain growth at high temperatures.

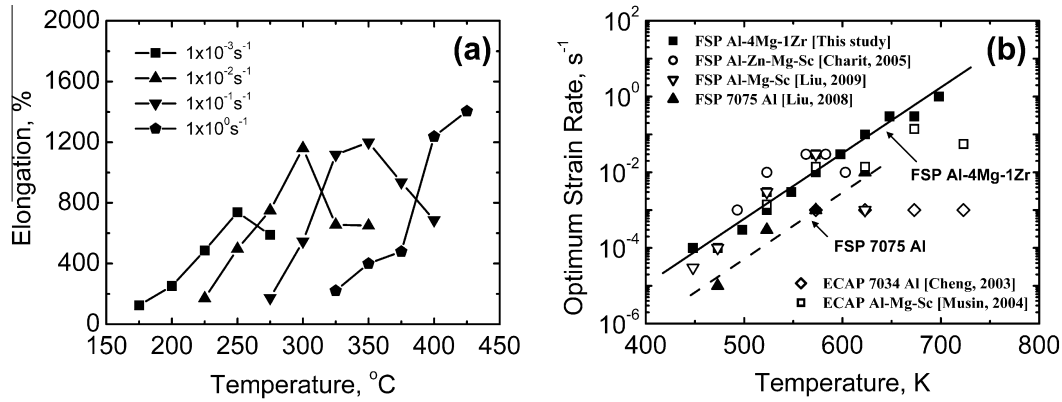


Fig. 11. (a) Variation of elongation with temperature for various strain rates and (b) variation of optimum strain rate for maximum superplasticity with temperatures for FSP Al-4Mg-1Zr and other UFG aluminum alloys.

The FSP UFG Al-4Mg-1Zr exhibited excellent thermal stability at high temperatures. Fig. 11a shows the variation of superplasticity with the testing temperature at various strain rates. It is noted that the optimum strain rate tended to increase with increasing temperature. In Fig. 11b, the optimum strain rate for maximum superplasticity is plotted as a function of temperature for the FSP Al-4Mg-1Zr. For the purpose of comparison, the superplastic data from other studies [20,21,23,38,43] are also included in this plot. It is clear that the optimum strain rate ( $\dot{\epsilon}_{\text{opti}}$ ) increased with increasing temperature ( $T$ ) for the FSP Al-4Mg-1Zr, which can be described as:

$$\log \dot{\epsilon}_{\text{opti}} = 0.0182T - 12.36. \quad (6)$$

This indicates that a linear relationship exists between  $\log \dot{\epsilon}_{\text{opti}}$  and  $T$ . For the present FSP Al-4Mg-1Zr, the actual grain sizes before deformation remained almost unchanged in the temperature range of 175–425 °C due to the effective pinning of numerous  $\text{Al}_3\text{Zr}$  particles on the grain boundaries (Figs. 3 and 4); therefore, the linear variation trend of  $\log \dot{\epsilon}_{\text{opti}}$  with  $T$  indicates a real effect of the temperature on the optimum strain rate. However, such a variation trend has not been reported in previous studies. This is due to the fact that for most fine-grained aluminum alloys, the grains exhibited an obvious coarsening with increasing temperature. At high temperatures, the actual grain sizes before superplastic deformation were much larger than the initial ones, which resulted in  $\log \dot{\epsilon}_{\text{opti}}$  deviating from the linear relationship with  $T$ . Fig. 11b clearly indicates that the superplastic data from other fine-grained aluminum alloys prepared by FSP or ECAP depart from the linear relationship at higher temperatures.

A similar relationship is also observed in Fig. 11b, indicated by a dashed line, for FSP 7075Al, whose superplastic data and microstructural evolution have been previously reported [23]. The equation is:

$$\log \dot{\epsilon}_{\text{opti}} = 0.0182T - 13.36. \quad (7)$$

This implies that the most possible relationship between  $\log \dot{\epsilon}_{\text{opti}}$  and  $T$  for superplasticity of the fine-grained aluminum alloys can be expressed as:

$$\log \dot{\epsilon}_{\text{opti}} = 0.0182T + B, \quad (8)$$

where  $B$  is a constant dependent on the material, grain size and grain boundary structure. It is well documented that reducing the grain size results in an increase in the optimum strain rate [14,37,38]. Furthermore, it has been suggested that the increase in the fraction of HAGBs is also beneficial in terms of increasing the optimum strain rate [14,15,20]. Fig. 11b indicates that, for a constant temperature, the optimum strain rate for the FSP Al-4Mg-1Zr is one order of magnitude higher than that for the FSP 7075Al, whereas for a constant optimum strain rate, the temperature for the former is 55 °C lower than that for the latter. This implies that it is easier to achieve HSRS and/or LTSP in the FSP Al-4Mg-1Zr than in the FSP 7075Al. Because the grain size usually exhibits a remarkable increase with increasing temperature for most of fine-grained aluminum alloys, the data that fit Eq. (8) are quite limited. Therefore, the validity and applicability of Eq. (8), need more supporting data. Furthermore, additional analysis is required to understand the physical meaning and implication of the slope of 0.0182 between  $\log \dot{\epsilon}_{\text{opti}}$  and  $T$ .

#### 4.3. Deformation mechanism

Identification of superplastic deformation mechanism depends on the precise evaluation of the parametric dependencies, i.e.  $n$ ,  $p$ ,  $Q$ , and the microstructural features after or during deformation. The surface observations of the deformed specimens have revealed evidence of GBS (Fig. 9). The grains were equiaxed and fine after superplastic deformation (Fig. 10). These indicate that GBS is the most plausible dominant deformation mechanism. The accommodation process of GBS would usually be the rate-controlling mechanism [44]. Quantitative models have been developed to describe GBS with accommodation by either diffusion or dislocation motion [45]. However, there is not an encompassing theory which is able to apply to all kinds of materials [45–47]. Phenomenological studies of a large variety of superplastic metallic materials have

revealed that they fall in two broad categories, characterized by either  $n = 2$  and  $Q = Q_L$  [48–50] or  $n = 2$ ,  $p = 2$  and  $Q = Q_{gb}$  [51–54], where  $Q_L$  and  $Q_{gb}$  are the diffusion activation energy in lattice and grain boundary, respectively. In order to establish the deformation model for FSP UFG aluminum alloys,  $n$ ,  $p$  and  $Q$  will be discussed in the following sections.

4.3.1. Threshold stress and true strain rate sensitivity

For the present FSP UFG Al–4Mg–1Zr, the  $m$  values tended to increase with increasing the strain rate in regions I and II over temperatures ranging from 175 to 425 °C. Similarly, the increase in the  $m$  value with the strain rate was observed in FSP fine-grained (1.5 μm) Al–4Mg–1Zr, though no region III was detected in this FSP sample [16]. This trend in the variation of the  $m$  value indicates that either a threshold stress was operative, or the deformation mechanism had changed. It has been suggested that lower  $m$  values in region I do not represent a genuine change in the rate-controlling mechanism, but rather originate from the existence of a threshold stress due to segregation of impurity atoms on the grain boundaries [55,56]. An analysis of the superplastic data of the FSP micro-grained Al–4Mg–1Zr revealed the existence of the threshold stresses [16]. If a threshold stress is responsible for the change in the  $m$  value, it can be determined when the deformation mechanism is known or assumed. The surface observation indicated that within the investigated temperature range, GBS is the most possible primary superplastic deformation mechanism. Furthermore, a very recent study indicated that GBS was the predominant deformation mechanism for FSP UFG Al–5.3Mg–0.23Sc even at 175 °C [24]

To determine the threshold stress, a plot of  $\sigma$  against  $\dot{\epsilon}^{1/n}$  ( $n = 1, 2, 3$  and  $5$ ) on double linear scales was adopted [57]. By using the superplastic data in regions I and II,  $n = 2$  gave the best linear fit among the assumed stress exponents

at all investigated temperatures. Therefore, all values of threshold stresses were estimated by an extrapolation of the data to zero strain rate with a linear regression, as illustrated in Fig. 12. The calculated threshold stresses are summarized in Table 2. The threshold stress values were highly dependent on the deformation temperature. Furthermore, the observed linear behavior on the plot of  $\sigma$  against  $\dot{\epsilon}^{1/2}$  indicates that the true  $m$  value is 0.5.

The origin of the threshold stress is not fully understood at the present time. Murty and Koczak [58] suggested that the threshold stress arose from the obstruction of grain boundary mobility by dispersed particles (Zener pinning) during superplastic flow at low stresses. Mohamed [57] suggested that the threshold stress resulted from the segregation of impurities at the grain boundaries and their interactions with grain boundary dislocations. Li and Langdon [59] suggested that the threshold stress originated from the inhibition of dislocation movement by dispersed particles and precipitates. These studies strongly suggest that the threshold stress in the FSP Al–4Mg–1Zr is associated with the high density of dispersed Al<sub>3</sub>Zr particles, which impeded the movement of the dislocations and grain boundaries during superplastic deformation.

4.3.2. True activation energy

The activation energy, which depends on a rate-controlling process, is also a very important factor in the determination of the deformation mechanism. The true activation energies evaluated according to the following equation [5] are shown in Fig. 13

$$Q_t = nR \frac{\partial[\ln(\sigma - \sigma_{th})]}{\partial(1/T)} \Big|_{\dot{\epsilon}} \tag{9}$$

The estimated activation energies under the constant strain rates are ~119–141 kJ mol<sup>-1</sup>. These values of  $Q_t$  are much higher than those for dislocation pipe diffusion in Al (82 kJ mol<sup>-1</sup>) and grain boundary diffusion in Al

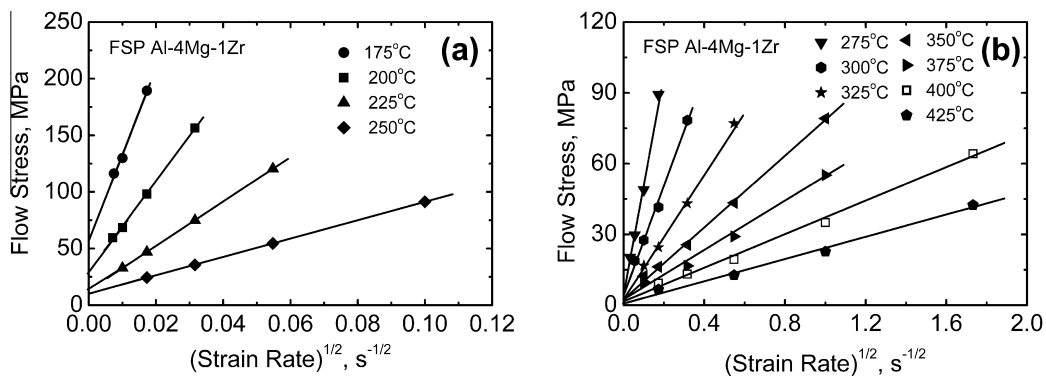


Fig. 12. Variation of flow stress as a function of  $\dot{\epsilon}^{1/2}$  for FSP Al–4Mg–1Zr.

Table 2  
Threshold stress of FSP Al–4Mg–1Zr at various temperatures.

Temperature (°C)	175	200	225	250	275	300	325	350	375	400	425
Threshold stress (MPa)	57.40	29.77	13.00	10.16	4.82	4.19	2.50	2.46	2.17	1.62	0.68

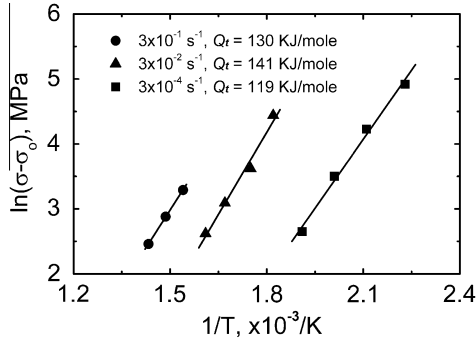


Fig. 13. Variation of  $\ln(\sigma-\sigma_0)$  as a function of reciprocal temperature for FSP Al-4Mg-1Zr.

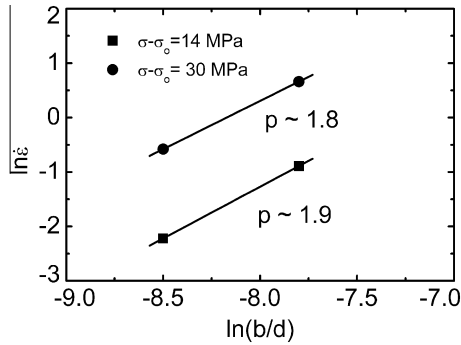


Fig. 14. Variation of  $\ln \dot{\epsilon}$  as a function of  $\ln(b/d)$  for FSP Al-4Mg-1Zr.

(84 kJ mol<sup>-1</sup>), and close to those for the Mg diffusion in the Al matrix (136 kJ mol<sup>-1</sup>) and lattice self-diffusion of pure Al (142 kJ mol<sup>-1</sup>).

It is well documented that the solute drag creep is a dominant deformation mechanism in coarse-grained Al-Mg alloys and in fine-grained Al-Mg alloys when deformed at low temperatures and high strain rates [60–64]. The solute drag creep is characterized by  $m$  values of 0.33 or smaller [61,62]. However, the apparent  $m$  value in the present study is generally higher than 0.33 and the modified  $m$  value is  $\sim 0.5$ . Thus, the solute drag creep might make a quite limited contribution to the observed superplasticity.

The most acceptable rate-controlling diffusion step might be the lattice diffusion of pure Al. Similarly, an activation energy value of 142 kJ mol<sup>-1</sup> was observed in the FSP UFG Al-Zn-Mg-Sc alloy [21]. The activation energy value will be further identified in Section 4.3.4.

#### 4.3.3. Grain size exponent

At a constant temperature ( $T$ ) and a normalized stress ( $\sigma-\sigma_0$ ), for discussion of the relationship between grain size and flow stress, Eq. (1) can be rewritten as:

$$\ln \dot{\epsilon} = A' + p \ln \left( \frac{b}{d} \right) + n \ln \left( \frac{\sigma - \sigma_0}{E} \right), \quad (10)$$

where  $A'$  is a temperature-dependent coefficient. The  $p$  value can be determined by finding the relationship between  $\dot{\epsilon}$  and  $d$  at a constant ( $\sigma-\sigma_0$ ) value. The superplastic data

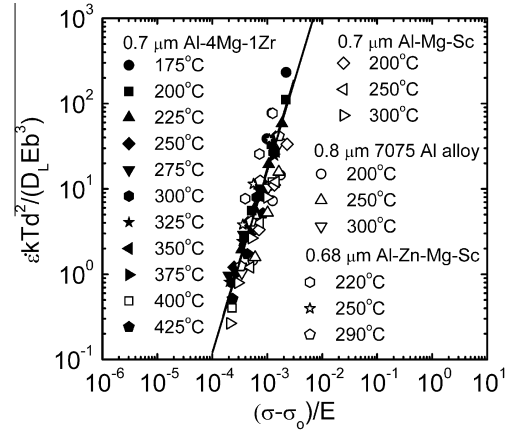


Fig. 15. Variation of  $(\dot{\epsilon}kTd^2/DLEb^3)$  as a function of  $(\sigma-\sigma_0)/E$  for FSP UFG aluminum alloys.

of the micrograined (1.5  $\mu\text{m}$ ) Al-4Mg-1Zr [16] were used in this study to determine the  $p$  value. The double linear plot of  $\ln \dot{\epsilon}$  against  $\ln(b/d)$  is presented in Fig. 14. The  $p$  value was determined to be close to 2.

#### 4.3.4. Constitutive equation for superplastic flow

To further elucidate the superplastic deformation mechanism in the FSP UFG Al-4Mg-1Zr, superplastic data are plotted in Fig. 15 as  $\dot{\epsilon}kTd^2/(DLEb^3)$  vs.  $(\sigma-\sigma_0)/E$ . It can be seen that all data for the FSP UFG Al-4Mg-1Zr fit onto a single straight line with a slope of 2 after introducing the threshold stress, showing that a threshold type deformation behavior with a stress exponent of 2 ( $\dot{\epsilon} \propto (\sigma-\sigma_0)^2$ ). The activation energy value, which is dependent on the rate-controlling process, is similar to the lattice self-diffusion of pure Al (142 kJ mol<sup>-1</sup>). The constitutive equation in the FSP UFG Al-4Mg-1Zr is given as:

$$\dot{\epsilon} = 5 \times 10^7 \frac{D_0 E b}{kT} \exp \left( -\frac{142000}{RT} \right) \left( \frac{b}{d} \right)^2 \left( \frac{\sigma - \sigma_0}{E} \right)^2. \quad (11)$$

This indicates that the dominant deformation mechanism for the FSP UFG Al-4Mg-1Zr is GBS controlled by the lattice diffusion.

For comparison, the data for the FSP UFG aluminum alloys from other studies [20,21,23] are also included in Fig. 15. At high temperatures, the actual grain sizes before superplastic deformation were much larger than the initial ones for these UFG alloys. Therefore, only the superplastic data obtained at  $\leq 300$  °C are added in this plot. It is clear that the present Al-4Mg-1Zr alloy behaved identically to other UFG superplastic aluminum alloys.

The constitutive equation for a nanocrystalline Al-Fe alloy is expressed by [49]:

$$\dot{\epsilon} = 1 \times 10^6 \frac{D_{eff} E b}{kT} \left( \frac{b}{d} \right)^2 \left( \frac{\sigma - \sigma_0}{E} \right)^2, \quad (12)$$

$$\text{where } D_{eff} = D_L + (1.7 \times 10^{-2})(\pi \delta d) D_{gb}. \quad (13)$$

The activation energy for the nanocrystalline Al-Fe alloy was 162 kJ mol<sup>-1</sup>, which is higher than that for the

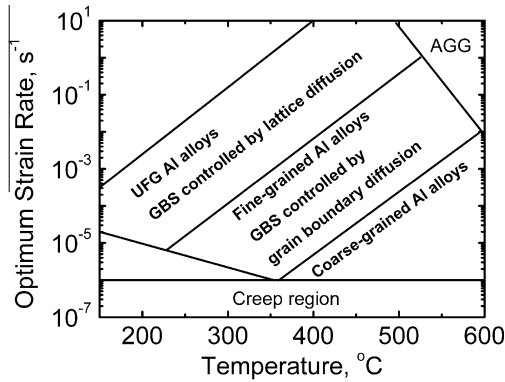


Fig. 16. A superplastic mechanism map for FSP aluminum alloys.

lattice diffusion of pure Al. Eq. (13) indicates that the contribution of  $D_L$  to  $D_{eff}$  decreased with decreasing temperature and grain size. This is not applicable to the FSP UFG aluminum alloys, whose activation energy value is similar to the lattice self-diffusion of pure Al.

#### 4.4. Superplastic mechanism map for FSP aluminum alloys

Eqs. 2, 8, and 11 and the reported superplastic data have made it possible to construct a superplastic mechanism map for the FSP aluminum alloys. Fig. 16 shows that the overall superplastic region is divided into three regions according to grain size. As discussed above, the constitutive equation for superplasticity in the FSP UFG aluminum alloys is expressed by Eq. (11). Therefore, in the UFG region, the dominant deformation mechanism is GBS controlled by the lattice diffusion. Eq. (2) is usually used to describe the superplastic flow of the FSP aluminum alloys with grains in the range of 1–10  $\mu\text{m}$  [14,16,18]. Thus, in the fine-grained region, the dominant deformation mechanism is GBS, which, however, is controlled by grain boundary diffusion. The transition line between the two regions depends on Eq. (8). Because of the lack of superplastic data of the FSP aluminum alloys with grains in the range of 0.8–1.5  $\mu\text{m}$  it is still hard to interpret the transition as a critical line corresponding to a well-defined grain size or as a region corresponding to a grain size range. Previous studies have indicated that the principal mechanism of superplasticity in coarse-grained Al–Mg alloys is solute drag on gliding dislocations [61]. Due to the lack of superplastic data for coarse-grained FSP aluminum alloys, the plastic deformation mechanism for these alloys at high temperatures is unknown. The AGG region is also shown in Fig. 16 based on the reported results. Reducing grain size usually decreased AGG to lower temperatures. Fig. 16 also indicates that grain refinement is beneficial for achieving superplasticity at higher strain rates and/or lower temperatures.

## 5. Conclusions

1. Al–4Mg–1Zr alloy with a grain size of 0.7  $\mu\text{m}$  prepared by FSP exhibited a boundary misorientation distribution

close to that for a random polycrystal. The ultrafine grains were very stable at elevated temperatures up to 425  $^{\circ}\text{C}$  due to the strong pinning effect of the high density of fine  $\text{Al}_3\text{Zr}$  particles.

2. The FSP Al–4Mg–1Zr exhibited superplasticity under the investigated temperature range of 175–425  $^{\circ}\text{C}$ . The optimum strain rate increased with increasing the temperature, as described in the form of  $\log \dot{\epsilon}_{\text{opti}} = 0.0182T - 12.36$ . Excellent high strain rate and low-temperature superplasticity of >1200% was observed at  $1 \times 10^{-2}$ – $1 \times 10^{-1} \text{ s}^{-1}$  for 300–350  $^{\circ}\text{C}$ . Even at 425  $^{\circ}\text{C}$ , a superplasticity of 1400% was achieved at an exceptionally high strain rate of  $1 \text{ s}^{-1}$ .
3. The surface observations of deformed specimens revealed distinct evidence of GBS at the investigated temperatures and strain rates. The analyses on the superplastic data of the UFG Al–4Mg–1Zr revealed the presence of a threshold stress for superplastic deformation, a stress exponent of 2, an inverse grain size dependence of 2, and an activation energy close to that for the lattice diffusion in Al. This indicates that the dominant deformation mechanism for the FSP UFG Al–4Mg–1Zr is GBS, which is controlled by lattice diffusion. Based on this notion, a constitutive equation was developed for the FSP UFG aluminum alloys in the form of  $\dot{\epsilon} = 5 \times 10^7 \frac{D_0 E b}{k T} \exp\left(-\frac{142000}{RT}\right) \left(\frac{b}{d}\right)^2 \left(\frac{\sigma - \sigma_0}{E}\right)^2$ .
4. A superplastic mechanism map for the FSP aluminum alloys was proposed. This map can be used as a guideline to design the FSP aluminum alloys with different grain sizes to obtain good superplasticity.

## Acknowledgements

Z.Y.M and F.C.L gratefully acknowledge the support of (a) the National Natural Science Foundation of China under grant nos. 50671103, 50871111 and 50890171, (b) the National Outstanding Young Scientist Foundation of China under grant no. 50525103, and (c) the Hundred Talents Program of Chinese Academy of Sciences. R.S.M gratefully acknowledges the support of the National Science Foundation through grants CMMI-0085044 and 0323725.

## References

- [1] Higashi K, Mabuchi M. Mater Sci Forum 1997;243–245:267.
- [2] Pu HP, Liu FC, Huang JC. Metall Mater Trans 1995;26A:1153.
- [3] McNelley TR, Crooks R, Kalu PN, Rogers SA. Mater Sci Eng 1993;A106:135.
- [4] Hsiao IC, Huang JC. Scripta Mater 1999;40:697.
- [5] Hsiao IC, Huang JC. Metall Mater Trans 2002;33A:1373.
- [6] Valiev RZ, Salimonenko DA, Tsenev NK, Berson PB, Langdon TG. Scripta Mater 1997;37:1945.
- [7] Ota S, Akamatsu H, Neishi K, Furukawa M, Horita Z, Langdon TG. Mater Trans 2002;43:2364.
- [8] Musin F, Kaibyshev R, Motohashi Y, Sakuma T, Itoh G. Mater Trans 2002;43:2370.

- [9] Berbon PB, Tsenev NK, Valiev RZ, Furukawa M, Horita Z, Nemoto M, et al. *Metall Mater Trans* 1998;29A:2237.
- [10] Mishra RS, Valiev RZ, McFadden SX, Islamgaliev RK, Mukherjee AK. *Philos Mag* 2001;81:37.
- [11] Noda M, Hirohashi M, Funami K. *Mater Trans* 2003;44:2288.
- [12] Tsuji N, Shiotsuki K, Saito Y. *Mater Trans JIM* 1999;40:765.
- [13] Mishra RS, Mahoney MW, McFadden SX, Mara NA, Mukherjee AK. *Scripta Mater* 2000;42:163.
- [14] Ma ZY, Mishra RS, Mahoney MW. *Acta Mater* 2002;50:4419.
- [15] Charit I, Mishra RS. *Mater Sci Eng* 2003;A359:290.
- [16] Ma ZY, Mishra RS, Mahoney MW, Grimes R. *Metall Mater Trans* 2005;36A:1447.
- [17] Ma ZY, Mishra RS, Mahoney MW. *Scripta Mater* 2004;50:931.
- [18] Johannes LB, Mishra RS. *Mater Sci Eng* 2007;A464:225.
- [19] Charit I, Mishra RS. *J Mater Res* 2004;19:3329.
- [20] Liu FC, Ma ZY, Chen LQ. *Scripta Mater* 2009;60:968.
- [21] Charit I, Mishra RS. *Acta Mater* 2005;53:4211.
- [22] Ma ZY, Mishra RS. *Scripta Mater* 2005;53:75.
- [23] Liu FC, Ma ZY. *Scripta Mater* 2008;58:667.
- [24] Liu FC, Ma ZY. *Scripta Mater* 2010;62:125.
- [25] Mukherjee AK, Bird JE, Dorn JF. *Trans Am Soc Met* 1969;62:155.
- [26] Bieler TR, Mukherjee AK. *Mater Sci Eng* 1990;A128:171.
- [27] Mishra RS, Bieler TR, Mukherjee AK. *Acta Metall Mater* 1995;43:877.
- [28] Mishra RS, Bieler TR, Mukherjee AK. *Acta Metall Mater* 1997;45:561.
- [29] Grimes R, Dashwood RJ, Harrison AW, Flower HM. *Mater Sci Technol* 2000;16:1334.
- [30] Dashwood RJ, Grimes R, Harrison AW, Flower HM. *Mater Sci Forum* 2001;357–359:339.
- [31] Mackenzie JK. *Biometrika* 1958;45:229.
- [32] Chen TR, Huang JC. *Metall Mater Trans* 1999;30A:53.
- [33] Perez-Prado MT, Gonzalez-Doncel G, Ruano OA, McNealley TR. *Acta Mater* 2001;49:2259.
- [34] Wang YN, Huang JC. *Scripta Mater* 2003;48:1117.
- [35] Liu FC, Ma ZY. *Scripta Mater* 2008;59:882.
- [36] Rabinovich MKh, Trifonov VG. *Acta Mater* 1996;44:2073.
- [37] Kaibyshev R, Avtokratova E, Apollonov A, Davies R. *Scripta Mater* 2006;54:2119.
- [38] Musin F, Kaibyshev R, Motohashi Y, Itoh G. *Scripta Mater* 2004;50:511.
- [39] Humphreys FJ, Hatherly M. *Recrystallization and related annealing phenomena*. Amsterdam: Elsevier; 2004. p. 109.
- [40] Humphreys FJ. *Acta Mater* 1997;45:5031.
- [41] Juul Jensen D. *Acta Mater* 1995;43:4117.
- [42] Doherty RD. *Met Sci* 1982;16:1.
- [43] Cheng X, Furukawa M, Horita Z, Langdon TG. *Acta Mater* 2003;51:6137.
- [44] Jiménez-Melendo M, Domínguez-Rodríguez A, Holgado-Salado M. *Int J Plasticity* 2001;17:341.
- [45] Edington JW, Melton KN, Cutler CP. *Prog Mater Sci* 1976;21:63.
- [46] Sherby OD, Wadsworth J. *Prog Mater Sci* 1989;33:169.
- [47] Nieh TG, Hsiung LM, Wadsworth J, Kaibyshev R. *Acta Mater* 1998;46:2789.
- [48] Langdon TG. *Phil Mag* 1970;22:689.
- [49] Somekawa H, Tanaka T, Sasaki H, Kita K, Inoue A, Higashi K. *Acta Mater* 2004;52:1051.
- [50] Hayden HW, Floreen S, Goodell PD. *Metall Trans* 1972;3A:833.
- [51] Gifkins RC. *Metall Trans* 1976;7A:1225.
- [52] Mukherjee AK. *Mater Sci Eng* 1971;8:83.
- [53] Arieli A, Mukherjee AK. *Mater Sci Eng* 1980;45:61.
- [54] Langdon TG. *Acta Metall Mater* 1994;42:2437.
- [55] Mohamed FA. *J Mater Sci* 1988;7:215.
- [56] Chaudhury PK, Mohamed FA. *Acta Metall* 1988;36:1099.
- [57] Mohamed FA. *J Mater Sci* 1983;18:582.
- [58] Murty GS, Koczak MJ. *Mater Sci Eng* 1988;100:37.
- [59] Li Y, Langdon TG. *Acta Mater* 1999;47:3395.
- [60] Yavari P, Langdon TG. *Acta Mater* 1982;30:2181.
- [61] Mcnelley TR, Michel DJ, Salama A. *Scripta Metall* 1989;23:1657.
- [62] Annekulas M, Green WP, Taleff EM, Krajewski PE, Mcnelley TR. *Metall Mater Trans* 2005;36A:1249.
- [63] Mcnelley TR, Ohishi K, Zhilyaev AP, Swaminathan SS, Krajewski PE, Taleff EM. *Metall Mater Trans* 2008;39A:50.
- [64] Soer WA, Chezhan AR, De Hosson JThM. *Acta Mater* 2006;54:3827.